Ab Initio thermodynamic and elastic properties of alkaline-earth metals and their hydrides

L. G. Hector, Jr. and J. F. Herbst
Materials and Processes Laboratory, GM R&D Center, Mail Code 480-106-224, 30500 Mound Road, Warren, Michigan 48090-9055, USA

W. Wolf and P. Saxe
Materials Design, P.O. Box 2000, Angel Fire, New Mexico 87710, USA

G. Kresse
Institute for Materials Physics, University of Vienna, Sensengasse 8/12, A-1090 Vienna, Austria
(Received 27 February 2007; revised manuscript received 4 April 2007; published 27 July 2007)

A systematic investigation of the alkaline earth hydrides BeH_2, MgH_2, CaH_2, SrH_2, BaH_2, the corresponding deuterides, and their antecedent metals is reported. We calculate lattice parameters, electronic and vibrational energies, enthalpies of formation at 0 and 298 K, components of the elasticity tensor, C_{ij}, and polycrystalline moduli based on the Hill criteria using density functional theory. Components of the Born effective charge tensors and phonon spectra are also computed for each hydride. We critically compare results obtained via the local density and generalized gradient approximations for the exchange-correlation energy functional. The volume dependence of the zero point energy is also investigated for Be and BeH_2.

DOI: 10.1103/PhysRevB.76.014121 PACS number(s): 61.50.Ah, 61.50.Lt, 62.20.Dc, 63.20.−e

I. INTRODUCTION

In addition to comprising a scientifically interesting class of materials, the binary alkaline earth hydrides are important components of hydrogen sorption-desorption reactions.[1–3] Of critical importance for predicting the thermodynamic stability of hydrides is the enthalpy of hydride formation, ΔH, which links the temperature and pressure of hydrogen sorption via the van't Hoff relation.[4] Previous theoretical studies of binary hydride stability have employed density functional theory[5] (DFT) to compute the electronic component, ΔH_{el}, of ΔH.[6,7] This requires approximations for the exchange-correlation functional, ε_{xc}, of which two are currently employed, viz., the local density approximation (LDA) and the generalized gradient approximation (GGA).[8] These approximations can lead to different equilibrium geometries and ΔH results, so that the choice of ε_{xc} can have significant impact on the accuracy of a calculation. In addition, many calculations neglect zero point effects, which are significant in the hydrogen molecule and may be in a solid hydride as well, and most experimental information corresponds to finite temperature while DFT is strictly appropriate only at 0 K. Although zero point and thermal effects may offset each other at a given temperature, thereby giving confidence in formation enthalpies predicted with electronic energies alone, their absence from the calculations raises questions about the predictive capability of DFT for new (i.e., hypothetical) materials.

Of the alkaline earth hydrides, MgH_2 has been the most extensively investigated in both the experimental and theoretical literature.[9,10] This is in part due to its hydrogen content of 7.6 mass %. MgH_2 has a relatively high formation enthalpy of −76 kJ/mol/H_2, however; this, together with its slow hydrogen sorption-desorption kinetics, currently preclude its use as a solid-state hydrogen storage material. Consequently, recent interest has turned to the addition of materials such as metals,[11–14] organics,[15] and carbon compounds[16] as possible destabilizing agents, and to mixing with other hydrides, such as Mg_2NiH_4.[17] Additional work has focused on altering MgH_2 morphology and surface properties by ball milling under various conditions.[18]

Motivated by the need to understand how ε_{xc} influences calculated elastic and thermodynamic properties, we compare LDA and GGA predictions of such properties for the alkaline earth metals (with the exception of radioactive radium) and their hydrides BeH_2, MgH_2, CaH_2, SrH_2, and BaH_2. Other than a report on LDA and GGA bulk and surface properties of Be and Mg,[19] we are not aware of such systematic comparisons in the literature. We have calculated electronic (0 K) and room temperature enthalpies of formation for the metals, the hydrides, as well as for the deuterides in the interest of completeness. We have also computed the elasticity tensor components, C_{ij}, using a least-squares fitting routine and derived bulk, shear and Young's moduli based on Hill's polycrystalline approximation for the metals (and compare with available experimental results) and hydrides (for which no measurements of elastic properties are available) using both functionals. Born effective charge tensor (BECT) components and electronic dielectric constants were also computed in ancillary calculations. The BECT components were used to model longitudinal optical-transverse optical (LO-TO) splittings in the hydride phonon dispersion curves. The effect of LO-TO splitting on computed room-temperature enthalpies of formation was investigated. It is anticipated that this knowledge will help guide selection of ε_{xc} for thermodynamic and mechanical property predictions of more complicated hydride systems.

II. COMPUTATIONAL APPROACH

All calculations in this study are based on density functional theory[5] as implemented in the Vienna *ab initio* simulation package (VASP) within a plane wave basis set.[20,21] Po-

tentials constructed by the projector-augmented wave (PAW) method were used for the elements.[22,23] The PAW procedure incorporates localized, atomic-like functions and plane waves; the former are required to vanish before overlapping with neighboring atoms. Consequently, the Hamiltonian matrix retains the simplicity of a plane wave basis without sacrificing the physics of localized functions. The core states remain fixed but the valence wave functions are updated during the computations. The ε_{xc} part of the density functional was treated within the LDA of Ceperley-Alder[24] as parametrized by Perdew-Zunger[25] and within the GGA of Perdew and Wang[26,27] in conjunction with the interpolation formula of Vosko *et al.*[28] The cutoff energies of the PAW potentials for elemental Be, Mg, Ca, Sr, Ba, and H were 308.45 (308.82), 265.57 (265.60), 150.00 (150.00), 226.33 (226.20), 186.98 (187.20), and 700.00 (700.00) eV in the LDA (GGA), respectively. All structural parameters (lattice constants and atom positions) of each studied material were optimized by simultaneously minimizing all atomic forces and stress tensor components via a conjugate gradient method.[29] Three successive full-cell optimizations (adapting basis vectors and computational grids to the cell parameters) were conducted to ensure that the cell energies and structural parameters were fully converged. Total energies were calculated by integration over a Monkhorst-Pack[30] mesh of *k*-points in the Brillouin zone with the linear tetrahedron method including Blöchl corrections[31] on the relaxed structures. For the metals $19\times19\times19$ *k*-meshes having 220 (400) points in the irreducible Brillouin zone were utilized for the hexagonal Be and Mg structures and fcc Ca and Sr (bcc Ba). $13\times13\times13$ meshes comprising 343 (196) irreducible wedge of the Brillouin zone *k*-points were employed for orthorhombic BeH_2, CaH_2, SrH_2, and BaH_2 (tetragonal MgH_2). The plane wave cutoff energy was 875 eV for each solid. In all cases, the total energy was converged to 10^{-7} eV/cell and the force components were relaxed to at least 10^{-4} eV/Å.

Phonon spectra for the solids, the vibrational frequency of the H_2 molecule, and the thermodynamic functions were computed by means of the direct approach to lattice dynamics,[32–34] with VASP as the computational engine. Discussions of the merits of this approach relative to the linear response and other methods are given in Refs. 35 and 36. The direct method involves construction of $N+1$ supercells: an unperturbed supercell and N perturbed supercells, where N is the number of crystallographically independent displacements of the constituent atoms. In each perturbed supercell, a single atom is displaced in a Cartesian direction in such a way that the N supercells explore all of the degrees of freedom of each symmetry-unique atomic site. In the present work, atomic displacements of ±0.01 Å were applied to the supercells (displacements up to ±0.03 Å were found to have no effect on the results). The supercell size was chosen such that interactions between equivalent atoms in periodic images were negligible, as were the computed force constants at the boundaries of each supercell. A $4\times4\times3$ supercell (96 atoms) was used for Be; $3\times3\times3$ supercells were constructed for Mg (54 atoms), Ca, and Sr (32 atoms); and a $2\times2\times2$ supercell (54 atoms) was used for Ba. For BeH_2 and MgH_2 $1\times3\times1$ ($Be_{36}H_{72}$) and $3\times3\times4$ ($Mg_{72}H_{144}$) supercells, respectively, were used. Phonon calculations on the remaining hydrides involved $2\times3\times1$ supercells ($M_{24}H_{48}$, M=Ca, Sr, Ba). Ancillary phonon calculations with larger supercells revealed no significant differences. For each of the $N+1$ supercells, the forces on all atoms were computed with VASP. Reciprocal space integration was performed by means of the Methfessel-Paxton technique[37] with a smearing width of 0.2 eV (the phonon results showed no sensitivity to small deviations in smearing width above and below 0.2 eV). From the *ab initio* forces obtained from each supercell, the force constant matrices were computed through a least-squares fit to the equation of motion of the lattice within the harmonic approximation. Fourier transformation of the force constants yielded the dynamical matrix, diagonalization of which provided phonon frequencies and eigenvalues for each selected q-point in reciprocal space. Integration over a large sample of q-vectors in the entire Brillouin zone yielded the phonon density of states from which the thermodynamic functions were computed. The force constants for each calculation were carefully examined to ensure that they became vanishingly small a few Å from each symmetry-unique displacement site, so that the point at which the force constants vanished was well within the boundaries of the corresponding supercell. The vibrational frequencies of H_2 and D_2 were computed with the same machinery by centering a single molecule in a $12\times13\times14$ Å^3 box.

In polar crystals ion core displacement creates an electric field that splits longitudinal and transverse optical phonon modes at the Γ-point. Since the field breaks the crystal symmetry, the LO-TO mode splitting cannot be directly computed by the direct approach based on supercells. The corresponding nonanalytical term in the dynamical matrix is taken into account, however, by making use of the BECT which describes the coupling between optical phonons and the electric field responsible for the splitting.[38] For MgH_2, CaH_2, SrH_2, and BaH_2 we explicitly compute the BECT using the linear response method recently implemented in VASP.[39] Although not pursued here, we note that an alternative approach involves evaluation of the Berry phase expression[40,41] (also in VASP[42]) for the change of polarization due to symmetry-independent displacements of atoms. Thermal expansion effects and the volume dependence of the zero point energy were neglected for all materials except Be and BeH_2, for which ancillary calculations are listed in the Appendix.

Components of the elasticity tensor, C_{ij}, for the crystalline materials were computed using the stress-based least-squares fitting method of LePage and Saxe.[43] This method, which recently resolved a discrepancy in the C_{14} elastic constant of α-Al_2O_3 (Ref. 44) and was applied to predict elastic constants of various hydride systems,[45,46] uses the stresses computed in the VASP code as inputs to a least-squares fit of the unknowns appearing in the equations describing the linear stress-strain relationships for a selected sequence of strains applied in various directions. Here, the unknowns are the three, five, six, and nine independent elastic constants for cubic, hexagonal, tetragonal, and orthorhombic symmetries, respectively, associated with the alkaline earth metals and their hydrides. The moduli are computed from the first derivatives of the stresses with respect to strain, rather than from the second derivatives of the total energy with respect

to strain (e.g., as in Ref. 47). Perhaps the most advantageous feature of the method is its full exploitation of symmetry, which makes for optimum computational efficiency. Tests were conducted with selected strains to determine the total number of strains necessary to minimize the least-squares errors for each computed C_{ij}. It was determined that application of six successive strains, viz., 0.5%, 0.6%, 0.7%, 0.8%, 0.9%, and 1.0%, was adequate to obtain $\leqslant 1\%$ statistical error in each computed C_{ij}. In addition, the quality of the least-squares fit, as gauged by the computed least-squares residual, was $\leqslant 1\%$ for all elastic constant calculations. The small residuals indicate that anharmonic effects due to the applied strains in the computed elastic constants are negligible. Tests with additional strains showed no significant deviation from the results reported here. Separate calculations with different k-point meshes were also conducted to determine the meshes needed to converge each C_{ij} to $\leqslant 0.5$ GPa. All calculations were performed on the primitive cell of each distorted structure.

III. H ATOM AND H_2 MOLECULE ENERGETICS

Calculations for the hydrogen atom and molecule were done with each centered in a $12\times13\times14$ $Å^3$ box, large enough to converge the energy without interaction effects from periodic images, using a plane wave cutoff energy of 960 eV. The PAW potentials lead to the H atom energies

$$E(\mathrm{H}) = -|E_{\mathrm{atom}}(\mathrm{H})| - E_{\mathrm{sp}} = \begin{cases} -12.5313\ \mathrm{eV} - 1.1209\ \mathrm{eV} \\ -12.1334\ \mathrm{eV} - 0.8967\ \mathrm{eV} \end{cases} = \begin{cases} -13.652\ \mathrm{eV\ GGA} \\ -13.030\ \mathrm{eV\ LDA} \end{cases}, \quad (1)$$

where the atomic reference energy $|E_{\mathrm{atom}}|$ is specified by the VASP potential file and the spin polarization energy E_{sp} was obtained from a spin-polarized atom-in-the-box computation. The exact (nonrelativistic) value is $E(\mathrm{H})=-13.606$ eV, from which our GGA (LDA) result differs by +0.046 (−0.576) eV. The total ground state energy of the molecule is

$$E^*(\mathrm{H_2}) = E(\mathrm{H_2}) - 2E_{\mathrm{atom}}(\mathrm{H}) = \begin{cases} -6.8016\ \mathrm{eV} - 25.0626\ \mathrm{eV} \\ -6.6989\ \mathrm{eV} - 24.2668\ \mathrm{eV} \end{cases} = \begin{cases} -31.864\ \mathrm{eV\ GGA} \\ -30.966\ \mathrm{eV\ LDA} \end{cases}, \quad (2)$$

where $E(\mathrm{H_2})$ is the total energy from the molecule-in-the-box calculation.[48] The GGA (LDA) result departs from $E^*(\mathrm{H_2})=-31.959$ eV obtained by Kolos and Roothaan[49] in a classic variational treatment by 0.095 eV=9 kJ/mole H_2 (0.99 eV =96 kJ/mol H_2). Our computed H_2 binding energy is

$$E_B(\mathrm{H_2}) = E^*(\mathrm{H_2}) - 2E(\mathrm{H}) = \begin{cases} -4.560\ \mathrm{eV\ GGA} \\ -4.905\ \mathrm{eV\ LDA} \end{cases}, \quad (3)$$

deviating by +0.19 (−0.16) eV in the GGA (LDA) from the −4.747 eV result (identical with experiment) in Ref. 49. The GGA (LDA) bond length is 0.749 (0.766) Å; Kolos and Roothaan[49] obtained 0.741 Å, equal to the measured value.

Aside from $E_B(\mathrm{H_2})$, the GGA provides a more accurate result for each quantity, in particular the H_2 ground state energy. $E(\mathrm{H_2})$ appears in our calculations of formation enthalpies ΔH for the hydrides. Since VASP has previously been shown to give results on a par with codes designed specifically for molecules,[50] we surmise that the largest source of error in these calculations is due to the approximate exchange-correlation functionals. Use of the same PAW potential and the same methodology in computing the total energy of each hydride and $E(\mathrm{H_2})$, however, makes for greater accuracy in ΔH due to cancellation of errors.

For the vibrational energy of the H_2 molecule, we obtain $\omega_0(\mathrm{H_2})=4243$ (4399) cm^{-1} in the LDA (GGA), so that the zero point energy is $\frac{1}{2}\hbar\omega_0(\mathrm{H_2})=25.4$ (26.3) kJ/mol H_2. The GGA frequency is in excellent agreement with the measured value of 4405 cm^{-1}.

IV. ALKALINE EARTH METALS

A. Structures and lattice optimization

The alkaline earth metals display a rich variety of physical properties over a range of pressures and temperatures. For example, crystalline Be and Mg are hexagonal close-packed structures with the $P6_3/mmc$ space group at 298 K. Above 1500 K, Be exhibits an hcp→bcc transition at atmospheric pressure, and a high pressure phase (12 GPa) has been identified.[51] Magnesium melts (922 K) at ambient pressure without a similar transition. At room temperature and pressures exceeding 50 GPa, Mg transitions to a bcc structure.[52] Unlike its alkaline earth counterparts, Be displays covalent character due to promotion of a $2s$ valence electron into an empty p state giving rise to sp hybridization.[53] In contrast, Mg is essentially a free-electron metal with a c/a ratio of 1.623 very near the ideal value $(8/3)^{1/2}=1.633$.

The properties of Ca, Sr, and Ba have attracted substantial interest in the theoretical community due to the transfer of electrons from free-electron-like s bands to more directional d bands at elevated pressures.[54] In fact, d-state hybridization is thought to be responsible for a substantial fraction of their cohesive energies.[55] Calcium and strontium are both fcc ($Fm\bar{3}m$) at room temperature and are semimetallic.[56] A Ca bcc phase occurs above 721 K and atmospheric pressure, or 20 GPa and room temperature.[57,58] Similarly, the bcc Sr phase occurs above 830 K and atmospheric pressure, or 4 GPa and room temperature.[58,59] Barium, which is bcc ($Im\bar{3}m$) from 0 K through melting, undergoes a complex sequence of pressure-induced phase transitions.[54] Electronic structure aspects of Be and Mg were investigated in Refs. 53 and 60, respectively, while the lattice dynamics of Be and Mg were addressed in Refs. 61 and 62, respectively. Electronic structure calculations for Ca and Sr are reported in Refs. 63–65 and Ref. 65, respectively, while Singh and Singh investigated the lattice dynamics of Ca and Sr.[66] The electronic structure of different phases of Ba was investigated in Refs. 65 and 67, while the lattice dynamics of Ba

TABLE I. Calculated (LDA, GGA) and experimental (room temperature) lattice constants a, c and atomic cell volumes V of the alkaline earth metals.

	Be hcp	Mg hcp	Ca fcc	Sr fcc	Ba bcc
			LDA		
a (Å)	2.23	3.13	5.30	5.77	4.76
c (Å)	3.53	5.06			
V (Å^3)	7.60	21.5	37.3	48.0	53.9
			GGA		
a (Å)	2.26 2.29[e]	3.19	5.49	5.97	4.99
c (Å)	3.57 3.58[e]	5.17			
V (Å^3)	7.91 8.07[e]	22.8	41.3	53.2	62.0
			Expt		
a (Å)	2.2858[a]	3.2089[b]	5.601[c]	6.076[d]	5.013[d]
c (Å)	3.5843[a]	5.2101[b]			
V (Å^3)	8.11	23.23	43.93	56.08	62.99

[a]Reference 69.
[b]Reference 70.
[c]Reference 71.
[d]Reference 72.
[e]Zero point contribution included.

was reported in Ref. 68. Since the alkaline earth metal phonon dispersion curves and densities of states from the present effort compare favorably with corresponding results in the literature, we do not elaborate on them here.

Room temperature experimental lattice constants and atomic coordinates for Be, Mg, and Ca were taken from Refs. 69–71, respectively, while those for Sr and Ba are from Ref. 72. The LDA and GGA PAW potentials for Be, Mg, Ca, Sr, and Ba were constructed with 4 ($1s^22s^2$), 8 ($2p^63s^2$), 8 ($3p^64s^2$), 10 ($4s^24p^65s^2$), and 10 ($5s^25p^66s^2$) valence electrons, respectively. The GGA and LDA computed lattice constants and volumes are compared with corresponding experimental values in Table I. We note that ε_{xc} has little effect on the predicted Be lattice constants as both functionals give results that compare favorably with the room temperature measurements listed in Table I. For the remaining metals, the GGA provides much better agreement with experiment. We furthermore note that the GGA usually has the tendency to overestimate equilibrium volumes, in particular for ionic and covalently bonded systems. Obviously, this does not apply to the alkaline earth metals which are (with some caveats) essentially free electron metals. The present gradient corrected functionals are designed to work well in this regime, a conjecture that our results clearly demonstrate to be the case.

B. Enthalpies of formation

The enthalpy of formation of a metal from its constituent atoms at temperature T can be written as

TABLE II. Calculated enthalpies of formation of the alkaline earth metals. Components of the values calculated in both the LDA and GGA are defined by Eq. (4). All entries in kJ/mol (=0.010 364 eV/atom).

	Be	Mg	Ca	Sr	Ba
			LDA		
E_{el}	−405.3	−169.5	−213.4	−181.5	−216.0
E_{ZPE}	9.4	3.1	2.2	1.3	0.9
ΔH_0	−396.0	−166.4	−211.2	−180.2	−215.0
$\delta\Delta H_{298}$	−4.4	−1.4	−0.7	−0.0	0.3
ΔH_{298}	−400.4	−167.8	−211.9	−180.2	−214.7
			GGA		
E_{el}	−358.0	−142.6	−184.5	−156.7	−185.6
E_{ZPE}	9.0	2.7	2.0	1.3	0.9
ΔH_0	−349.0	−139.9	−182.5	−155.5	−184.7
$\delta\Delta H_{298}$	−4.3	−1.2	−0.5	+0.0	0.4
ΔH_{298}	−353.3	−141.1	−183.1	−155.4	−184.3
			Expt		
ΔH_0 expt[a]	−320	−145.90	−177.3	−164.4	−179.8
ΔH_{298} expt[a]	−324	−147.10	−177.8	−164.0	−179.1

[a]Reference 73.

$$\begin{aligned}\Delta H_T &= (E+pV)_{\text{metal}} - (E+pV)_{\text{atom}} \\ &\approx (-|E_{\text{atom}}| + E_{\text{el}} + E_{\text{ZPE}} + E_{\text{ph}}) \\ &\quad - \left(-|E_{\text{atom}}| + \tfrac{5}{2}kT\right) \\ &= (E_{\text{el}} + E_{\text{ZPE}}) + \left(E_{\text{ph}} - \tfrac{5}{2}kT\right) \\ &\equiv \Delta H_0 + \delta\Delta H_T. \end{aligned} \quad (4)$$

Here, E_{atom} is the total atomic energy; E_{el} is the VASP-optimized total energy of the metal, specified with respect to the reference energy $|E_{\text{atom}}|$; E_{ZPE} is the zero point energy of the metal; E_{ph} is the phonon contribution (without the ZPE) to the energy of the metal at T; and $\frac{5}{2}kT$ is the sum of the translational energy $\frac{3}{2}kT$ and $pV=kT$ for the atom assuming the ideal gas law. pV for the metal has been ignored since the small molar volume makes pV insignificant at $p=1$ bar. No spin polarization terms appear since the alkaline earth atoms all have $^1S_0$ ground states and the metals are all nonmagnetic. $\Delta H_0 \equiv E_{\text{el}} + E_{\text{ZPE}}$ is the $T=0$ formation enthalpy or, equivalently, the (negative of the) cohesive energy; $\delta\Delta H_T \equiv E_{\text{ph}} - \frac{5}{2}kT$ is the change to temperature T.

Table II lists E_{el}, E_{ZPE}, ΔH_0, $\delta\Delta H_{298}$, ΔH_{298}, and experimental enthalpies of formation. The largest impact of the ε_{xc} choice is on E_{el}; E_{ZPE} and E_{ph} are nearly equal in the LDA and GGA. It is quite clear from Table II that the GGA results are in much more favorable agreement with experiment. Among Mg, Ca, Sr, and Ba the greatest discrepancy between the GGA value of ΔH_{298} and the corresponding measured value is 5% for Sr. Magnesium (beryllium) is characterized by the least negative (most negative) enthalpy of formation as a consequence of its free-electron (covalent) nature. ΔH_{298} for Be in the GGA deviates from experiment by 9%. The fact

that our GGA results for the other metals are in significantly better accord with experiment might suggest that the measurement for Be is the least accurate among those in Table II. This is not appropriate, however, since the covalent contribution in Be is stronger than in the other materials, and hence the GGA is expected to work less reliably.

C. Elastic constants and related moduli

Single-crystal elastic constants, C_{ij}, calculated for the five alkaline earth metals considered here are listed in Table III along with other theoretical predictions and available experimental data. Each C_{ij} was calculated at the theoretical equilibrium volume. Great care was taken in the choice of a k-point mesh for each calculation since the C_{ij} depend sensitively on the mesh density. For Be and Mg a mesh with 400 symmetry-unique k-points was used for the unstrained structure. The subsequent calculations involved five distortions about the unstrained lattice, with the lowest symmetry ($C2/m$) structure requiring 1810 symmetry-unique k-points. For Ca, Sr, and Ba a mesh with 220 symmetry-unique k-points was found to achieve the desired energy convergence for the unstrained structures. The ensuing calculations involved three distorted structures, the least symmetric of which (*Immm* for Ca and Sr; *Fmmm* for Ba) requiring 1000 symmetry-unique k-points. Following Ref. 46, we refer to the C_{ii} ($i \leqslant 3$) as longitudinal, the C_{ii} ($i \geqslant 4$) as shear, and the C_{ij} ($i \neq j \leqslant 3$) as off-diagonal components of the elasticity tensor.

Voigt-Reuss-Hill estimates B_{VRH}, G_{VRH}, and Y_{VRH} of the polycrystalline bulk (B), shear (G), and Young's (Y) moduli were computed from the C_{ij} (definitions can be found in Ref. 85), and the Debye temperature Θ was then estimated from them following the procedure detailed in Ref. 45. Table III also contains these quantities as well as selected experimental and other theoretical results. Direct measurements of the C_{ij} are only available for Be and Mg.

Due to its covalent bond character, Be is the most resistant to longitudinal and shear distortions: its C_{ii} are all markedly greater than those for the other metals, as Table III shows. Interestingly, only the computed C_{13} for the other hcp metal, Mg, exceeds that of Be in either the LDA or GGA, an observation that is supported by experiment. C_{11} and C_{12} decrease from Be to Ba in either approximation for $\varepsilon_{\mathrm{xc}}$ while C_{44} for Ca exceeds that of Mg, but is less than the computed C_{44} for Sr. Ba is the least resistant to shear distortion. In general, the C_{ij} obtained in the LDA exceed the corresponding GGA values due to LDA overbinding. The same holds true for the polycrystalline moduli, B_{VRH}, G_{VRH}, Y_{VRH}, and Θ. The GGA/LDA values of each decrease monotonically from Be to Ba following the experimental trends noted in Table III for both the single crystal and polycrystalline moduli. For Be, the LDA C_{11}, C_{13}, and the GGA C_{33}, C_{44} are closest to experiment. The notable exceptions are the LDA/GGA C_{12} moduli which are far greater than the reported experimental values. The Be G_{VRH}, Y_{VRH}, and Θ from LDA are for the most part closer to the corresponding polycrystalline values from experiment than those in the GGA, with the marked exception of the polycrystalline bulk (B_{VRH}) modulus. LDA C_{ii} and the GGA $C_{i\neq j}$ are in better accord with experiment for Mg; the single, marginal departure is C_{33} (Mg), for which the GGA result is slightly closer to the measured value. The LDA G_{VRH} and Y_{VRH} and the GGA B_{VRH} and Θ for Mg are closer to experiment. For Ca, both the LDA and GGA C_{11} and C_{44} values agree well with one of the two reported experimental values for each. The LDA C_{12} value for Ca is closer to both experimental values listed in Table III than the GGA C_{12} value. For Sr, the GGA C_{11}, C_{44}, B_{VRH}, G_{VRH} and the LDA C_{12}, Y_{VRH} are closest to experiment, while for Ba the GGA C_{11}, C_{44}, Y_{VRH} and the LDA C_{12}, B_{VRH} are closest to experiment.

V. ALKALINE EARTH HYDRIDES

A. Structures and lattice optimizations

The structure of BeH_2 is body-centered orthorhombic (*Ibam*) with 12 BeH_2 formula units (f.u.) per conventional cell.[86] It consists of an array of corner-sharing BeH_4 tetrahedra linked by H atoms. Electronic structure and vibrational properties of BeH_2 were reported in Refs. 87 and 88, respectively. While all the binary alkaline earth hydrides are insulators, BeH_2 is unique in that it is the only hydride with covalent, as opposed to ionic bond character. At sufficiently high pressures, however, the bonding in BeH_2 is predicted to change from covalent to ionic.[87]

Magnesium hydride is tetragonal (space group $P4_2/mnm$, rutile structure), and its bonding (as revealed from electronic structure studies) is primarily ionic with no covalent character.[9] The conventional cell comprises two f.u., and the H atoms form a minimally distorted hcp lattice with Mg atoms occupying 50% of the octahedral sites. Structural transitions in MgH_2 were investigated in Ref. 89. The rutile form was found to transform to an orthorhombic *Pbmn* structure at 0.39 GPa. At 3.84 GPa, the *Pbmn* structure transforms to a *Pnma* structure, also orthorhombic, and at 6.7 GPa a $Pbc2_1$ structure forms. At sufficiently high pressures, MgH_2 exhibits metallic character.

The electronic structure of CaH_2 was investigated in Ref. 90 using the Hartree-Fock method, and those of SrH_2 and BaH_2 were investigated in Refs. 91 and 92, respectively, using local basis sets and pseudopotentials. Each hydride is an ionic insulator, with the *Pnma* (orthorhombic) space group, in which the metal atoms are surrounded by nine H atoms in a packing that approximates hcp ($PbCl_2$-type structure). Each cell contains four formula units. VASP-computed GGA (LDA) band gaps are BeH_2: 5.496 eV (4.662 eV); MgH_2: 3.965 eV (3.555 eV); CaH_2: 3.105 eV (2.816 eV); SrH_2: 3.221 eV (2.812 eV); and BaH_2: 2.901 eV (2.745 eV). Although no band-gap measurements are readily available for the alkaline earth hydrides, we note that DFT typically underestimates band-gap values relative to experiment.

Table IV presents our calculated lattice constants and experimental information. For the Mg, Ca, Sr, and Ba materials measurements on both the hydrides and deuterides exist in the literature and indicate no marked isotope effects.[86,93–99] It is clear that the computed results (0 K) in the GGA are in excellent agreement with experiment (room temperature) and

TABLE III. Elastic constants C_{ij} calculated for the alkaline earth metals, polycrystalline moduli B_{VRH}, G_{VRH}, Y_{VRH}, and Debye temperatures Θ derived from them, and corresponding experimental and previous theoretical results. All C_{ij} and moduli in GPa.

	Be (hcp)	Mg (hcp)	Ca (fcc)	Sr (fcc)	Ba (bcc)
			LDA		
C_{11}	285.1	66.0	24.2	18.5	13.8
C_{12}	70.8	31.2	16.2	12.7	8.8
C_{13}	11.7	23.7			
C_{33}	418	71.6			
C_{44}	174	16.1	17.2	17.8	11.8
B_{VRH}	130.2	40	18.9	15	10
G_{VRH}	145.9	18	9.7	9	6
Y_{VRH}	318.5	47	24.6	22	16
Θ (K)	1366.1	431	225.6	189	129
			GGA		
C_{11}	259.6	59.3	22.5	15.4	11.9
C_{12}	69	25.8	14.3	10.8	7.5
C_{13}	10.7	21.0			
C_{33}	391.6	61.6			
C_{44}	166.4	14.2	14.8	14.9	10.3
B_{VRH}	120.7	35	17	12	9
G_{VRH}	134.8	16	8.9	7	6
Y_{VRH}	294.6	42	22.6	18	14
Θ (K)	1322.4	413	219.7	176	123
			Previous theory		
C_{11}		59.43[d]	26.65,[e] 18.63,[f] 19.2[g]	18.88,[f] 6.1[g]	12.1[f]
C_{12}		25.60[d]	16.19,[e] 17.71,[f] 16.4[g]	14.73,[f] 15.9[g]	16.7[f]
C_{13}	10,[a] −3[b]	21.40[d]			
C_{33}	420,[a] 390[b]	61.64[d]			
C_{44}	172[c]	16.42[d]	17.04,[e] 15.09,[f] 16.0[g]	11.80,[f] 14.9[g]	16.3[f]
B_{VRH}		35[d]	20,[e] 18,[f] 17[g]	16,[f] 16[g]	15[f]
B	140,[a] 120[b]		19.68,[e] 18.02[f]		15.2[f]
G_{VRH}		17[d]	11,[e] 5,[f] 7[g]	6,[f] 5[g]	1[f]
G			10.41[f]		9[f]
Y_{VRH}		45[d]	27,[e] 13,[f] 17[g]	16,[f] 12[g]	−2[f]
			Experiment		
C_{11}	299.4,[h] 293.6[i]	63.48[h]	27.8,[j] 22.8[k]	15.3[l]	12.6[l]
C_{12}	27.6,[h] 26.8[i]	25.94[h]	18.2,[j] 16.0[k]	13.6[l]	11.1[l]
C_{13}	11.0,[h] 14.0[i]	21.70[h]			
C_{33}	342.2,[h] 356.7[i]	66.45[h]			
C_{44}	166.2,[h] 162.2[i]	18.42[h]	16.3,[j] 14[k]	9.9[l]	9.5[l]
B_{VRH}	115,[h] 117[i]	37[h]	21,[j] 18[k]	17[l]	12[l]
B	100,[m] 116.8[i]	35[m]	15,[m] 18.3,[k,n] 18.7[n]	12[m]	10,[m] 9.4[n]
G_{VRH}	152,[h] 150[i]	19[h]	10,[j] 8[k]	8[l]	4[l]
G	143,[m] 150.1[i]	17[m]	7[m]	5[m]	5[m]
Y_{VRH}	318,[h] 315[i]	49[h]	26,[j] 21[k]	21[l]	10[l]
Y	298,[m] 315.2[i]	44[m]	20[m]	14[m]	13[m]
Θ (K)	1367,[m] 1453[i]	363[m]	208[m]	133[m]	97[m]

[a]Reference 74; LDA.
[b]Reference 74; GGA.
[c]Reference 75; first principles pseudopotential method.
[d]Reference 76; first principles pseudopotential method.
[e]Reference 77; resonant model potential.
[f]Reference 78; model potential.
[g]Reference 66.
[h]Reference 79.
[i]Reference 80; 295 K.
[j]Reference 81; inferred from measured phonon dispersion curves; 300 K.
[k]Reference 57; inferred from measured phonon dispersion curves; 300 K.
[l]Reference 82; inferred from measured phonon dispersion curves; 293 K.
[m]Reference 83.
[n]Reference 84.

TABLE IV. Calculated and (room temperature) experimental lattice constants a, b, and c and cell volumes V (per formula unit) of the alkaline earth hydrides.

	BeH_2 orth	MgH_2 tet	CaH_2 orth	SrH_2 orth	BaH_2 orth
			LDA		
a (Å)	8.63	4.43	5.70	6.16	6.59
b (Å)	3.91	4.43	3.47	3.77	4.08
c (Å)	7.43	2.97	6.58	7.13	7.69
V (Å^3)	20.92	29.16	32.61	41.32	51.69
			GGA		
a (Å)	8.95 9.17[e]	4.50	5.88	6.35	6.84
b (Å)	4.12 4.20[e]	4.50	3.56	3.85	4.16
c (Å)	7.63 7.78[e]	3.01	6.75	7.29	7.87
V (Å^3)	23.46 24.98[e]	30.53	35.30	44.54	55.93
			Expt		
a (Å)	9.082[a]	4.5025[b]	5.995[c]	6.361[c]	6.789[d]
b (Å)	4.160	4.5025	3.598	3.857	4.171
c (Å)	7.707	3.0123	6.806	7.303	7.852
V (Å^3)	24.26	30.53	36.70	44.79	55.59

[a]Reference 86.
[b]Reference 93; $Mg(D_{0.9}H_{0.1})_2$.
[c]Reference 94; deuterides.
[d]Reference 95; BaD_2.
[e]Zero point contribution included.

superior to those in the LDA. Most of the theoretical values in Tables I and IV were obtained by minimizing the electronic total energies E_{el} alone, raising the fundamental question of the impact of zero point effects. In the Appendix, we explore this issue for Be and BeH_2, the lightest materials considered here and those for which such effects will be most pronounced, via calculations of the volume dependence of the zero point energy, $E_{ZPE}(V)$. We find that the ZPE contribution increases the calculated cell volume for Be (BeH_2) by 1.9% (6.6%); the results are listed in Tables I, IV, and XIII. It can be anticipated that the influence of $E_{ZPE}(V)$ on the lattice parameters of the heavier metals and their hydrides is significantly smaller.

B. Dielectric properties, vibrational spectra, and zero point energies

Long-range Coulomb forces can arise when a nonmetallic crystal is deformed so that the dielectric properties, described by the Born effective charge tensor (BECT) and the dielectric constants, may influence other properties such as phonon dispersion. In particular, splittings of the longitudinal optical (LO) and transverse optical (TO) phonon modes can be introduced.

We have computed BECTs with the linear response method. The components of the BECT can be calculated by determining the first order change of the wave functions for an electric field E_α and then, using the chain rule, the second derivative of the total energy with respect to both E_α and the ionic positions. Alternatively, the first order change in the wave functions with respect to the ionic positions can be determined, and the BECT deduced from the microscopic change in the polarization; this also corresponds to the second derivative of the total energy with respect to E_α and the ionic positions, but with the chain rule applied in the opposite order. Both approaches have been implemented recently in VASP and yield the same values within a fraction of a percent. The first order variation of the wave functions with E_α and the required commutator of the Hamiltonian with the position operator (i.e., the velocity operator) are discussed for the PAW method in Ref. 102.

We designate the BECT as $Z^*_{\tau,\alpha\beta}$ where τ specifies a particular atom and α, β are Cartesian directions, and we denote the formal valence of atom τ by Z_τ. Calculation of the full BECT necessitates displacement of each atom in each Cartesian direction. For sites of high symmetry the required number of calculations can be reduced; in the case of tetragonal MgH_2, for example, displacements in the x and z directions are sufficient.

LDA and GGA components of $Z^*_{\tau,\alpha\beta}$ computed for BeH_2 are listed in Table V, those for MgH_2 in Table VI and those for CaH_2, SrH_2, and BaH_2 are given in Table VII. Except for BeH_2, the diagonal components do not depart substantially from the formal valence Z_τ. For BeH_2, however, some diagonal charge tensor elements are reduced down to a third of the nominal charge value, and for MgH_2 and BeH_2 large off-diagonal elements of up to 0.3 are obtained. Component-by-component comparison reveals only minor differences between the LDA and GGA. Our GGA results for MgH_2 compare very favorably with those of Ohba *et al.*[10] based upon the Perdew, Burke, and Ernzerhof GGA,[103] as Table VI shows.

The components of the high frequency dielectric constant tensor, ε_∞, were calculated including local field effects using the linear response method as implemented in VASP[102] and are listed in Table VIII. In addition, we computed ε_∞ for LiH as a check against the experimental value of 3.61.[104] Our GGA (LDA) value is 4.35 (5.01), in reasonable proximity to previous calculations using a density functional approach with pseudopotentials which yielded ε_∞ ranging from 4.81 to 5.93.[105] While no measurements for the alkaline earth hydrides are available, we anticipate that, as for LiH, our GGA results will be closer to experiment than the LDA values. Our $\varepsilon^{xx}_\infty = 3.91$, $\varepsilon^{zz}_\infty = 3.96$ results for MgH_2 in the GGA agree very well with the corresponding 3.90 and 3.93 values obtained by Ohba *et al.*[10]

Figures 1–5 display computed phonon dispersion curves, with LO-TO splittings, along selected high symmetry paths and total phonon densities of states for each hydride. Only results from the GGA are presented since the LDA curves did not reveal any essential differences. No imaginary modes appeared in any of the calculations. Figures 1(a) and 1(b) for BeH_2 show a spectrum of frequencies that is wider than any of the other materials, both consequences of the covalent

TABLE V. Components of the Born effective charge tensor calculated for body-centered orthorhombic BeH_2 in the LDA and GGA.

BeH_2	*xx*	*yy*	*zz*	*xy*	*yx*	*yz*	*zy*	*xz*	*zx*
					LDA				
Be1	1.09	0.80	1.24	0	0	0	0	0	0
Be2	1.08	1.00	1.03	0.22	−0.18	0	0	0	0
H1	−0.52	−0.34	−0.66	−0.09	−0.05	0.09	0.08	0.23	0.22
H2	−0.59	−0.73	−0.33	−0.23	−0.25	0	0	0	0
					GGA				
Be1	1.23	0.82	1.36	0	0	0	0	0	0
Be2	1.20	1.13	1.15	0.27	−0.20	0	0	0	0
H1	−0.58	−0.37	−0.74	−0.09	−0.06	0.09	0.08	0.27	0.26
H2	−0.65	−0.80	−0.36	−0.30	−0.32	0	0	0	0

bonding. The phonon bands in BeH_2 occur in three well-defined groups. At the zone center in the GGA, we find 12 modes in the 1885–2066 cm^{-1} range (upper), 12 modes in the 1039–1407 cm^{-1} range (middle), and 30 modes in the 0–828 cm^{-1} range (lower). Splitting of the lowest (highest) bands in the upper (middle) ranges are evident. The vibrations in the upper range correspond to out-of-phase scissors and stretching motions of H atoms in the BeH_4 tetrahedra. Modes in the middle range are due to stretching of a majority of
the H atoms along the *a* axis with comparatively small vibrations of the Be atoms. The lowest frequency vibrations (<800 cm^{-1}) are complicated mixtures of H atom stretching, rocking, and scissoring, with the amplitude of oscillation of the Be atoms noticeably larger. Yu *et al.*[88] calculated the lattice dynamics of BeH_2 using a central force Born-von Karman model. They also found three major groups of modes, but in the frequency ranges 2140–2380, 1140–1400, and 0–880 cm^{-1}. The differences with our results stem from their use of force constants extracted from calculations for H absorbed on a Be (0001) surface and a cluster model for BeH_2, which clearly tends to overestimate the stiffness of the Be-H bonds.

TABLE VI. Components of the Born effective charge tensor calculated for tetragonal MgH_2 in the LDA and GGA.

MgH_2	*xx*	*zz*	*xy*
		LDA	
Mg	1.83	1.92	0.11
H	−0.91	−0.96	−0.21
		GGA	
Mg	1.86	1.95	0.12
H	−0.93	−0.98	−0.22
		Ohba *et al.*[a] GGA	
Mg	1.85	1.93	0.12
H	−0.92	−0.96	−0.21

[a]Reference 10.

In Fig. 2(a) for MgH_2, the solid dots represent Raman data;[106] MgH_2 is the only hydride considered here for which such data are available. Our GGA results compare favorably with those of Ohba *et al.*[10] The highest frequency at the zone center, 1462 cm^{-1}, is substantially lower than that for BeH_2, 2380 cm^{-1}, and dispersion is clearly more pronounced in MgH_2. Both observations are consistent with the fact that MgH_2 is an ionic insulator with a heavier metal atom. Figure 2(b) shows that the vibrational frequencies fall roughly into five bands centered at approximately 1430, 1200, 1020, 600, and 200 cm^{-1}. Along the zone center, H stretching modes in the *ab* plane appear in the uppermost band, while H stretches along the *c* axis occur near 1000 cm^{-1}. At 519 cm^{-1}, H stretching modes appear in the *bc* plane. At 295 cm^{-1}, H and Mg stretching modes appear in the *ab* plane at 45° relative to the *a* axis. At 281 cm^{-1}, H ions exhibit a rocking motion about stationary Mg ions. At 183 cm^{-1}, H and Mg stretching modes appear in the bc plane with motion parallel to the *c* axis.

The spectra for CaH_2, SrH_2, and BaH_2 in Figs. 3–5 are qualitatively very similar and feature three groups of modes. The highest frequencies at the zone centers for CaH_2, SrH_2, and BaH_2 as predicted with the GGA are 1174, 1076, and 1012 cm^{-1}, respectively. These correspond to stretching of H atoms in the *ac* plane of each structure. At intermediate frequencies H oscillation along the *b* axis dominates. In the lowest band, rocking of the metal atoms along with H atoms in the *ac* plane is dominant.

Table IX contains the zero point energies (ZPEs) we computed with and without the LO-TO zone splittings. The influence of the splittings on the ZPEs is clearly minimal, with the largest effect ~0.2 kJ/mol for MgH_2 in either the LDA or GGA. For comparison, we derived ZPEs for the alkaline earth deuterides as well (also listed in Table IX). The phonon spectra from which they were obtained were computed without LO-TO splittings and, aside from an overall compression of the energy scales, resemble the hydride spectra in Figs. 1–5. The larger mass of deuterium leads to smaller ZPEs; in fact, the difference between a hydride ZPE divided by $\sqrt{2}$ and its corresponding deuteride ZPE in Table IX varies by only 3%–7%. Furthermore, in both the LDA and the GGA the ZPE decreases with the mass of the metal atom, as does

TABLE VII. Components of the Born effective charge tensor calculated for orthorhombic CaH_2, SrH_2, and BaH_2 in the LDA and GGA.

	xx	*yy*	*zz*	*xz*	*zx*
			LDA		
			CaH_2		
Ca	1.85	1.82	1.94	0.12	−0.01
H1	−0.92	−0.84	−0.97	−0.04	−0.03
H2	−0.93	−0.99	−0.97	−0.06	−0.03
			SrH_2		
Sr	1.90	1.87	1.98	0.12	0.00
H1	−0.95	−0.86	−0.99	−0.04	−0.03
H2	−0.95	−1.01	−0.99	−0.06	−0.02
			BaH_2		
Ba	2.02	2.01	2.14	0.17	0.03
H1	−1.01	−0.91	−1.08	−0.05	−0.03
H2	−1.01	−1.10	−1.05	−0.06	−0.02
			GGA		
			CaH_2		
Ca	1.95	1.93	2.01	0.09	−0.02
H1	−0.95	−0.89	−1.00	−0.05	−0.03
H2	−1.00	−1.04	−1.01	−0.05	−0.03
			SrH_2		
Sr	1.99	1.97	2.04	0.09	−0.01
H1	−0.97	−0.91	−1.02	−0.04	−0.02
H2	−1.01	−1.05	−1.02	−0.05	−0.02
			BaH_2		
Ba	2.10	2.09	2.19	0.14	0.03
H1	−1.02	−0.96	−1.11	−0.05	−0.03
H2	−1.08	−1.13	−1.08	−0.05	−0.01

the difference between a hydride ZPE and its deuteride cognate.

C. Enthalpies of formation

Enthalpies of hydride formation ΔH are vital since they control the equilibrium H_2 pressure p and temperature T of the hydriding reaction $M+H_2 \leftrightarrow MH_2$ via the van't Hoff relation[4]

$$\ln p/p_0 = \Delta H/RT - \Delta S/R, \tag{5}$$

where ΔS is the entropy change (largely due to H_2), p_0 is unit H_2 pressure, and R is the gas constant. First principles calculations of ΔH have been reported for a number of binary hydrides[6,7] as well as for the ternary systems $LaNi_5H_7$ (Ref. 45), Mg_2NiH_4 (Refs. 107 and 108), RCo_5H_4 (R=La,Pr; Ref. 109), $LiNH_2/Li_2NH$ (Ref. 101), and several Na-Al-H phases.[110] Smithson *et al.*[6] calculated electronic enthalpies of formation (ΔH_{el} as defined below) for BeH_2, MgH_2, CaH_2, SrH_2, and BaH_2 using VASP with ultrasoft pseudopotentials in the LDA, and Wolverton *et al.*[7] reported similar calculations for the Mg, Ca, Sr, and Ba hydrides in the GGA.

Proceeding as in Sec. IV B and again ignoring pV for the metals, we write the enthalpy $H=E+pV$ for each constituent at $T=0$ as

$$H_0 + E_{el} + E_{ZPE}, \tag{6}$$

where E_{el} is the electronic total energy and E_{ZPE} the zero point energy ($=\frac{1}{2}\Sigma_{\vec{q}}\hbar\omega_{\vec{q}}$ for the solids, $\frac{1}{2}\hbar\omega_0$ for H_2, and ω

TABLE VIII. Components of the high frequency [ion clamped (Ref. 39)] dielectric constant tensor ε_∞ calculated for the alkaline earth hydrides.

	BeH_2	MgH_2	CaH_2	SrH_2	BaH_2
			LDA		
ε_∞^{xx}	3.91	4.25	4.81	4.45	4.76
ε_∞^{yy}	3.86	4.25	4.67	4.33	4.64
ε_∞^{zz}	3.74	4.30	5.05	4.62	4.91
			GGA		
ε_∞^{xx}	3.36	3.91	4.42	4.07	4.25
ε_∞^{yy}	3.18	3.91	4.33	3.99	4.17
ε_∞^{zz}	3.26	3.96	4.57	4.18	4.37

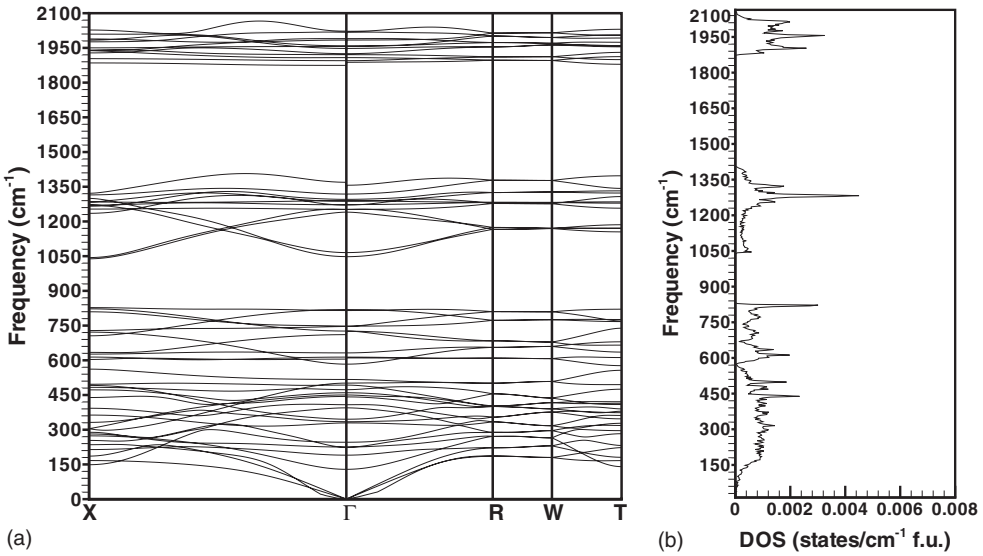

FIG. 1. GGA PAW phonon dispersion relations (a) and total phonon densities of states (DOS) (b) for BeH_2 calculated with LO-TO splitting.

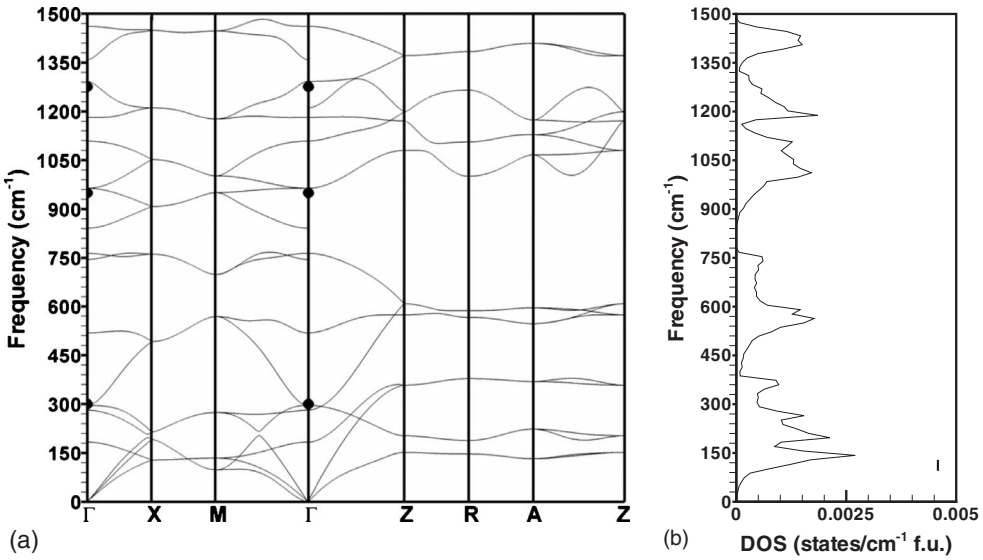

FIG. 2. GGA PAW phonon dispersion relations (a) and total phonon densities of states (DOS) (b) for MgH_2 calculated with LO-TO splitting. The solid dots represent Raman data from Ref. 106.

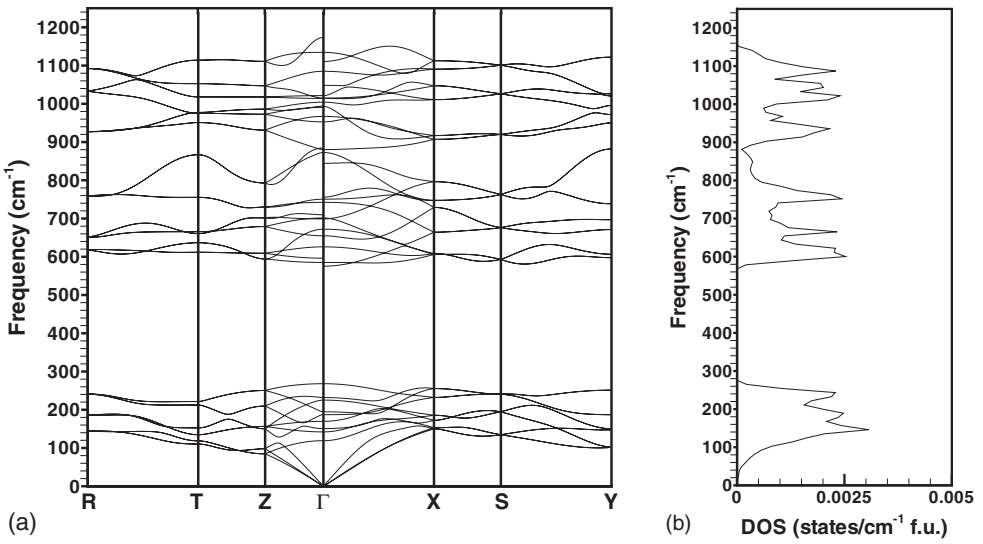

FIG. 3. GGA PAW phonon dispersion relations (a) and total phonon densities of states (DOS) (b) for CaH_2 calculated with LO-TO splitting.

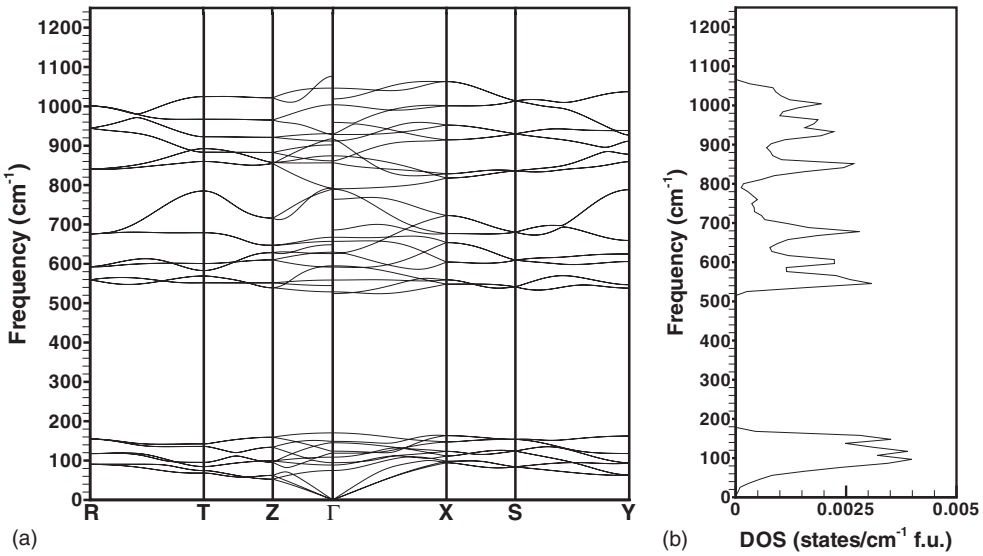

FIG. 4. GGA PAW phonon dispersion relations (a) and total phonon densities of states (DOS) (b) for SrH_2 calculated with LO-TO splitting.

the vibrational frequencies). The $T=0$ enthalpy of formation ΔH_0, using MgH_2 as an example, can then be written as the sum of electronic and ZPE components:

$$\begin{aligned}\Delta H_0(\mathrm{MgH_2}) &\equiv \Delta H_{\mathrm{el}} + \Delta H_{\mathrm{ZPE}} \\ &= [E_{\mathrm{el}}(\mathrm{MgH_2}) - E_{\mathrm{el}}(\mathrm{Mg}) - E_{\mathrm{el}}(\mathrm{H_2})] \\ &\quad + [E_{\mathrm{ZPE}}(\mathrm{MgH_2}) - E_{\mathrm{ZPE}}(\mathrm{Mg}) - E_{\mathrm{ZPE}}(\mathrm{H_2})].\end{aligned} \tag{7}$$

To obtain H at finite T we add the phonon energy (without the ZPE) $E_{\mathrm{ph}}=\Sigma_{\vec{q}}\hbar\omega_{\vec{q}}n(\omega_{\vec{q}})$, $n(\omega)=(e^{\hbar\omega/kT}-1)^{-1}$, to H_0 of each solid and the translational $(\frac{3}{2}kT)$, rotational (kT), $pV=kT$, and vibrational $E_{\mathrm{vib}}=\hbar\omega_0 n(\omega_0)$ energy to H_0 of each H_2 molecule and write

$$\Delta H_T = \Delta H_0 + \delta\Delta H_T. \tag{8}$$

For MgH_2 specifically, we have

$$\delta\Delta H_T(\mathrm{MgH_2}) = E_{\mathrm{ph}}(\mathrm{MgH_2}) - E_{\mathrm{ph}}(\mathrm{Mg}) - \left[\tfrac{7}{2}kT + E_{\mathrm{vib}}(\mathrm{H_2})\right]. \tag{9}$$

Our computed enthalpies of formation are listed in Table X along with available experimental results. The LDA values for ΔH_0, and hence ΔH_{298}, are all substantially more negative than the corresponding GGA results, again reflecting the tendency of the LDA to bind more strongly. The ZPE component ΔH_{ZPE} in the LDA is 1–3 kJ/mol H_2 larger than in the GGA, but for both $\varepsilon_{\mathrm{xc}}$ it decreases monotonically from BeH_2 to BaH_2. $\delta\Delta H_{298}$ behaves differently, exhibiting a minimum for CaH_2 in the LDA and GGA. Irrespective of $\varepsilon_{\mathrm{xc}}$ CaH_2 is predicted to be the most stable of the five hydrides and BeH_2 the least stable, as is the case experimentally. In all instances, the LDA and GGA ΔH_{298} results bound the measured values. On the quantitative side the GGA ΔH_{298} are in better agreement with experiment, except for MgH_2; the fact that they are all less negative than the measurements is indicative of the GGA's occasional tendency to underbind for metal-gas reactions. Our ΔH_{el} in the GGA are in good accord

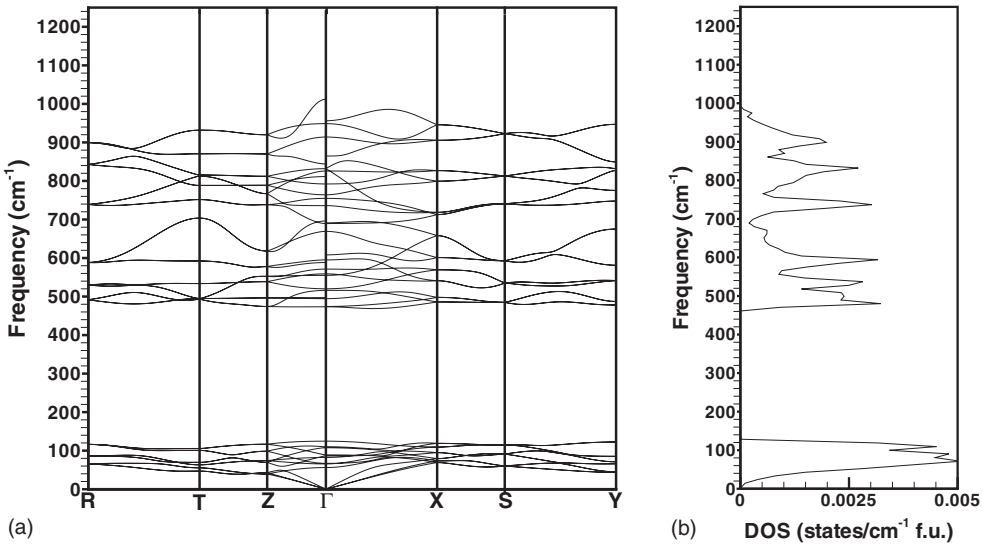

FIG. 5. GGA PAW phonon dispersion relations (a) and total phonon densities of states (DOS) (b) for BaH_2 calculated with LO-TO splitting.

TABLE IX. Alkaline earth hydride (deuteride) LDA/GGA zero point energies with and without LO-TO splittings. All values in kJ/mol H_2 (D_2).

	LDA		GGA	
Hydride (deuteride)	No LO-TO splitting	LO-TO splitting	No LO-TO splitting	LO-TO splitting
BeH_2 (BeD_2)	52.34 (39.94)	52.37	51.98 (39.58)	52.11
MgH_2 (MgD_2)	39.60 (29.38)	39.83	38.90 (28.82)	39.08
CaH_2 (CaD_2)	35.61 (26.33)	35.69	33.71 (24.90)	33.81
SrH_2 (SrD_2)	31.51 (23.02)	31.59	29.74 (21.72)	29.83
BaH_2 (BaD_2)	27.74 (20.16)	27.82	26.08 (18.96)	26.17

with those of Wolverton *et al.*,[7] while the departures of the LDA values from those of Smithson *et al.*[6] are somewhat larger; the differences can be ascribed mostly to our use of PAW potentials here versus ultrasoft pseudopotentials in Refs. 6 and 7. We see from Table X that, although ΔH_{el} in the GGA (LDA) for BeH_2, CaH_2, SrH_2, BaH_2 (MgH_2) provides a reasonable approximation to the measured ΔH_{298}, the agreement is improved by the addition of $[\Delta H_{\mathrm{ZPE}}+\delta\Delta H_{298}]$ in each case.

Also listed in Table X are ΔH_{298} results derived excluding the LO-TO splittings in the phonon dispersion relations. The effect of the splittings on ΔH_{298} is at most 0.1 kJ/mol H_2 (for BeH_2 and MgH_2 in the GGA), demonstrating that they can be safely neglected in calculating enthalpies of formation. This is because (i) E_{ZPE} is an integral over all the phonon energies and is thus insensitive to the details of $\omega_{\vec{q}}$ in a rather small fraction of the Brillouin zone and (ii) at 298 K only modes with small $\omega_{\vec{q}}$ are of importance to E_{ph}.

TABLE X. Enthalpies of formation for the alkaline earth hydrides. Components of the values calculated in both the LDA and GGA are defined by Eqs. (10)–(13). ΔH_{298} results computed without LO-TO splittings are also listed. All entries in kJ/mol H_2.

	BeH_2	MgH_2	CaH_2	SrH_2	BaH_2
			LDA		
	−42.8	−87.8	−220.5	−204.6	−182.2
ΔH_{ZPE}	17.6	11.4	8.1	4.9	1.5
ΔH_0	−25.2	−76.4	−212.4	−199.7	−180.7
$\delta\Delta H_{298}$	−6.4	−8.0	−8.5	−8.0	−7.4
ΔH_{298}	−31.5	−84.6	−221.0	−207.8	−188.2
ΔH_{298} (No LO-TO splitting)	−31.5	−84.6	−221.0	−207.8	−188.2
			GGA		
ΔH_{el}	−25.1	−62.2	−173.8	−165.2	−149.3
ΔH_{ZPE}	16.8	10.1	5.5	2.3	−1.0
ΔH_0	−8.3	−52.1	−168.3	−162.9	−150.3
$\delta\Delta H_{298}$	−6.5	−8.1	−8.3	−7.7	−7.1
ΔH_{298}	−14.8	−60.3	−176.7	−170.7	−157.6
ΔH_{298} (No LO-TO splitting)	−14.9	−60.4	−176.7	−170.7	−157.6
			Expt		
ΔH_0		−68.00[b]			
ΔH_{298}	−18.86[a]	−76.15[b]	−188.8,[c] −181.5[d]	−177,[c] −180.3[d]	−171.5,[c] −177.0[d]

[a]Reference 111.
[b]Reference 73.
[c]Reference 112.
[d]Reference 113.

TABLE XI. Enthalpies of formation for the alkaline earth deuterides; LO-TO splittings were neglected. $|\Delta|$ is the magnitude of the difference between ΔH_{298} values for a deuteride and the corresponding hydride (from Table X). All values in kJ/mol D_2.

	BeD_2	MgD_2	CaD_2	SrD_2	BaD_2
			LDA		
ΔH_{el}	−42.8	−87.8	−220.6	−204.6	−182.2
ΔH_{ZPE}	12.6	8.3	6.1	3.7	1.2
ΔH_0	−30.2	−79.5	−214.4	−200.9	−181.0
$\delta\Delta H_{298}$	−5.5	−6.8	−7.2	−6.5	−5.8
ΔH_{298}	−35.7	−86.3	−221.6	−207.4	−186.8
$\|\Delta\|$	4.2	1.7	0.6	0.4	1.4
			GGA		
ΔH_{el}	−25.1	−62.2	−173.8	−165.2	−149.3
ΔH_{ZPE}	12.2	7.8	4.5	2.1	−0.3
ΔH_0	−12.9	−54.5	−169.2	−163.1	−149.6
$\delta\Delta H_{298}$	−5.5	−6.9	−6.9	−6.1	−7.1
ΔH_{298}	−18.4	−61.4	−176.1	−169.2	−156.7
$\|\Delta\|$	3.6	0.9	0.6	1.5	0.9
			Expt		
ΔH_0					
ΔH_{298}	−30[a]				

[a]Reference 111.

We also derived ΔH for the alkaline earth deuterides following Eqs. (6)–(9) but with E_{ZPE} and E_{ph} obtained from vibrational calculations for the deuterides and the D_2 molecule. The same crystal structures were assumed, and LO-TO splittings were not included. Our retention of the electronic terms E_{el} for the hydrides and H_2 is in keeping with the Born-Oppenheimer approximation. Electronic structure codes quite generally ignore the finite mass of the nucleus since it would have a miniscule effect on E_{el}. One measure of the error associated with this approximation is given by the 0.3 kJ/mol larger ionization energy of the deuterium atom compared to that of the hydrogen atom. The impact on ΔH is even smaller since ΔH involves energy differences. Employing the same cell as for H_2, we obtained $E_{ZPE}(D_2)$ = 18.02(18.38) kJ/mol D_2 in the LDA (GGA); the experimental value is 18.65 kJ/mol D_2.[114] The systematics of ΔH_{298} for the deuterides in Table XI are similar to those of the hydrides in Table X. CaD_2 (BeD_2) is the most (least) stable independent of the choice of ε_{xc}. ΔH_{ZPE} diminishes uniformly from BeD_2 to BaD_2, and for BaD_2 its sign in the GGA is reversed from that in the LDA, as is also the case for BaH_2 in Table X. A measured enthalpy of formation is available only for BeD_2.[111] In contrast to the case for BeH_2, $\Delta H_{298}(BeD_2)$ in the LDA is in better agreement with the measurement than the GGA value. Given the fact that the LDA and GGA $\Delta H_{298}(BeD_2)$ bracket experiment, as we found for all of the hydrides (Table X), we anticipate that our LDA and GGA ΔH_{298} results will bound experiment for the other deuterides as well. Table XI shows, in accord with expectation, that the largest differences between our ΔH_{298} values for the deuterides and corresponding hydrides occurs for the Be materials, the lightest members of the series.

D. Elastic moduli and elastic stability

Elastic constants calculated for the five alkaline earth hydrides are listed in Table XII along with Hill polycrystalline moduli and Debye temperatures derived as in Sec. IV C for the metals. For the unstrained orthorhombic Ibam BeH_2 structure 343 *k*-points were selected. Nine subsequent distortions generated structures with the *Ibam*, *C*2/*c*, and *C*2/*m* space groups, with the latter two resulting from shear distortions and requiring substantially denser *k*-meshes. A total of 54 geometry optimizations were demanded by the chosen strain set. For the hexagonal $P4_2/mnm$ space group of MgH_2 196 *k*-points were adequate for convergence. Six subsequent distortions produced *Pnnm*, $P4_2/mnm$, $P2_1/c$, and *Cmmm* structures, the latter two again from shear distortions, and 36 geometry optimizations were required. For the orthorhombic Pnma structure of CaH_2, SrH_2, and BaH_2, a mesh of 343 *k*-points was also chosen; nine symmetry-unique distortions led to structures with the *Pnma*, $P2_1/c$, and $P2_1/m$ space groups, and 54 geometry optimizations were required to compute the elastic constants.

Both the LDA and GGA indicate that CaH_2 is stiffest along the *a* and *b* axes since its C_{11} and C_{22} values exceed those for the other hydrides. In contrast, MgH_2 is stiffest along the *c* axis as suggested by its extreme C_{33} value. Moreover, MgH_2 exhibits the greatest resistance to shear distortions in the *bc* and *ab* planes since its C_{44} and C_{66} moduli, respectively, are the largest. Of the orthorhombic hydrides, BeH_2 and CaH_2 are the most resistant to shear distortion in the *ac* plane due to their large C_{55}. The LDA predicts the largest values of the Hill polycrystalline moduli for CaH_2, whereas the GGA predicts the same for MgH_2. The covalent nature of BeH_2 is the origin of its large Debye temperature. The Θ values systematically decrease from BeH_2 to BaH_2 in either the LDA or GGA; this is not surprising since larger values of Θ are associated with stronger interatomic forces and lighter atoms.

Unlike the situation for the alkali metals, no measured elastic constants are available in the literature for the hydrides. We can compare our results, however, with those of other calculations, all of which employed theoretical methods significantly different from the approach used here. MgH_2 was treated in the Hartree-Fock (HF) approximation,[115] and some of the elastic constants were extracted from the lattice parameter dependence of total energies obtained via a pseudopotential technique.[9] A Hartree-Fock-linear combination of atomic orbitals (HF-LCAO) scheme with various Gaussian basis sets was used for CaH_2 (Refs. 90 and 91) and SrH_2.[91] For MgH_2 the values of ($C_{11}+C_{12}$), C_{13} in Refs. 9 and 114 and C_{33} in Ref. 115 are in reasonable agreement with our results for either ε_{xc}, but C_{33}=100 GPA in Ref. 9 and C_{44}=171 GPa, C_{66}=22 GPa in Ref. 115 depart substantially from our C_{33}=138.9 (131.9) GPa, C_{44}=40.2 (38.5) GPa, and C_{66}=56.3 (52.3) GPa in the LDA (GGA). In Table XII the ranges for

TABLE XII. Calculated elastic constants C_{ij}; polycrystalline moduli B_{VRH}, G_{VRH}, and E_{VRH}; and Debye temperatures Θ of alkaline earth hydrides. All C_{ij} and moduli in GPa.

	BeH_2	MgH_2	CaH_2	SrH_2	BaH_2
			LDA		
C_{11}	85.3	77.3	95.1	69.3	45.7
C_{12}	5.3	39.2	27.3	24.2	23.4
C_{13}	13.9	32.6	28.6	25.1	22.6
C_{22}	66.4		111.3	86.6	65.9
C_{23}	4.2		37.6	33.4	30.5
C_{33}	101.6	138.9	113.7	87.7	64.1
C_{44}	24.7	40.2	37.7	28.3	21.2
C_{55}	41.7		41.5	30.3	19.9
C_{66}	30.0	56.3	40.5	28.8	18.9
B_{VRH}	32.6	54.5	56.0	44.9	35.7
G_{VRH}	33.8	37.4	38.9	28.1	18.4
E_{VRH}	75.4	91.2	94.9	69.8	47.2
Θ (K)	1143.4	870.4	700.8	430.1	298.4
			GGA		
C_{11}	69.8	73.1	91.1	69.1	50.0
C_{12}	0.3	33.9	18.9	16.1	14.9
C_{13}	10.7	20.4	24.8	21.3	18.8
C_{22}	44.9		98.4	77.6	59.6
C_{23}	0.5		29.7	25.8	22.9
C_{33}	91.1	131.9	99.6	77.6	58.7
C_{44}	17.5	38.5	29.0	22.5	17.2
C_{55}	35.6		36.7	28.0	19.9
C_{66}	24.4	52.3	34.2	24.6	16.6
B_{VRH}	24.3	50.2	48.3	38.8	31.0
G_{VRH}	27.1	36.1	34.2	25.6	18.1
E_{VRH}	59.3	87.3	82.9	63.0	45.5
Θ (K)	1044.8	854.8	664.2	413.1	293.8
			Other calculations		
$C_{11}+C_{12}$		107,[a] 110[b]			
C_{11}			13.5–22.9[c]	31.3–37.8[c]	
C_{12}			109.2–126.7[c]	85.5–90.3[c]	
C_{13}		22,[a] 30[b]	66.7–85.4[c]	104.1–114.8[c]	
C_{22}			74.2–84.6[c]	37.8–46.1[c]	
C_{23}			135.2–162.5[c]	101.5–109.5[c]	
C_{33}		139,[a] 100[b]	30.2–44.0[c]	56.2–62.7[c]	
C_{44}		171[a]	112.7–124.6[c]	45.2–67.8[c]	
C_{55}			88.5–108.3[c]	61.8–77.1[c]	
C_{66}		22[a]	81.5–97.4[c]	55.6–58.5[c]	
B		49,[a] 49[b]	190.1–226.8[c]	161.5–180.4[c]	

[a]Reference 115.
[b]Reference 9.
[c]Reference 91; Table III.

the C_{ij} from Ref. 91 arise from the various orbital basis sets explored; it is quite obvious that there are many extreme disparities with our findings. In particular, the single crystal bulk moduli B from Ref. 91 are, respectively, 190–227 (161–180) GPa for CaH_2 (SrH_2). These are a factor of ~4 larger than our B_{VRH} values and are ~50% of the measured B=443 GPa for diamond,[116] which has the highest known bulk modulus; the method employed here yields B_{VRH} (diamond)=439 GPa.[117] We infer that the C_{ij} reported in Refs. 90 and 91 require further scrutiny.

As a qualitative check we assessed the mechanical stability of each hydride in Table XII by diagonalizing the C_{ij} matrix and evaluating the Born stability criteria.[118] For each of our ten sets of C_{ij}, we find that the eigenvalues are all positive, confirming mechanical stability in the absence of applied stress (cf. Ref. 119). This is in agreement with the

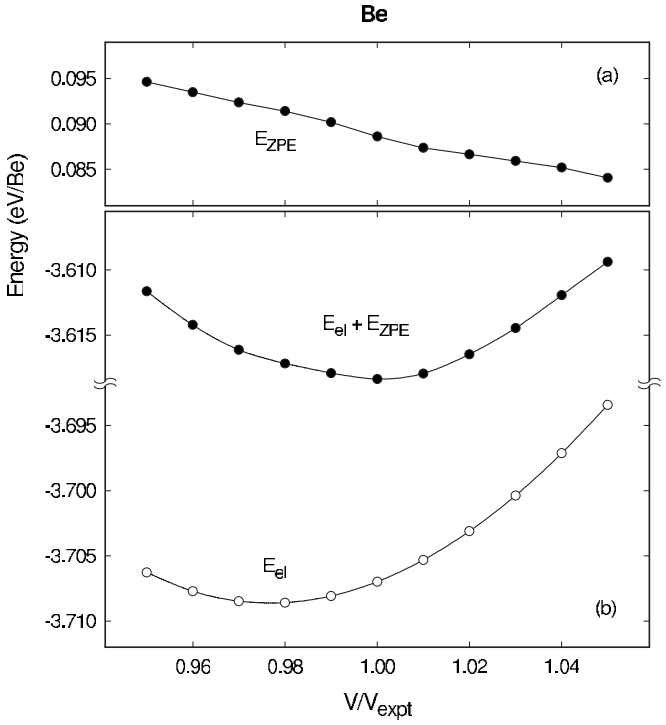

FIG. 6. Electronic and zero point energies E_{el}, E_{ZPE} calculated as functions of volume V in the GGA for Be.

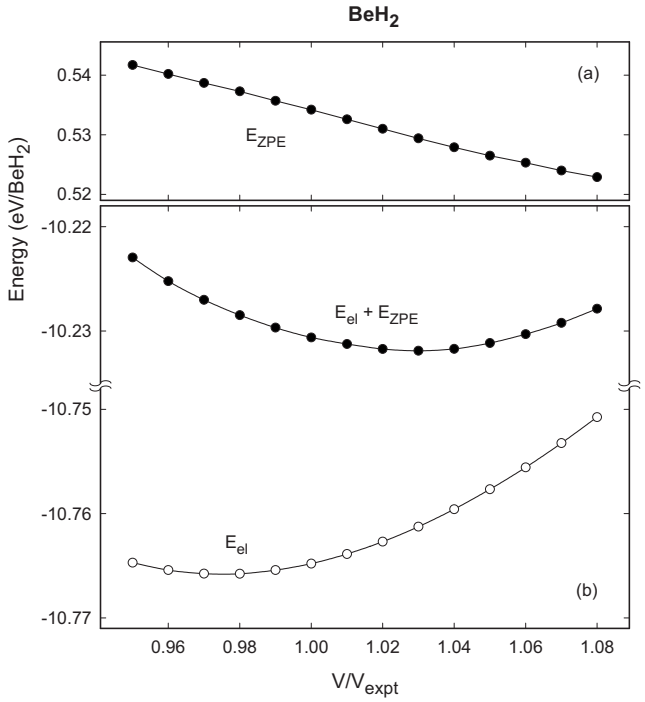

FIG. 7. Electronic and zero point energies E_{el}, E_{ZPE} calculated as functions of volume V in the GGA for BeH_2.

fact that the lowest frequency acoustic branches at the Γ-point in the phonon dispersion plots of Figs. 1–5 all have positive slopes. On the other hand, each of the eight sets of C_{ij} in Ref. 91 for CaH_2 and SrH_2 yields two large, negative eigenvalues, indicating elastic instability.

VI. REMARKS

We have explored the effect of the exchange-correlation energy functional ε_{xc} on thermodynamic, dielectric, and elastic properties of the alkaline earth hydrides and their parent metals via calculations in both the LDA and GGA using a state-of-the-art DFT method. Although it is common to find the GGA employed in the extant literature on metallic and complex hydrides, often with minimal justification, our goal was to compare predictions from both functionals with available experimental data for a technologically significant and rather well-characterized class of hydrides.

Electronic total energies E_{el} are most affected by the ε_{xc} choice, with the LDA generally leading to larger binding energies than the GGA. Phonon spectra and, hence, zero point energies and finite temperature lattice energies are much less sensitive to ε_{xc}, as are the components of the BECT for the hydrides. This was evident from the observation that computed vibrational spectra in the LDA and GGA revealed no essential differences. The lattice constants obtained by minimizing E_{el} in the GGA are generally in better accord with experiment for all the materials considered here with the possible exception of Be. The GGA also yields room temperature enthalpies of formation ΔH_{298} that are in more favorable agreement with measurements than the LDA values, with the conspicuous exception of MgH_2. Consequently, the selection of ε_{xc} is particularly important for Mg-based hydrides, a class of materials of significant current interest. The fact that the LDA and GGA results for ΔH_{298} bound the measured values for all the hydrides suggests a useful metric for assessing the accuracy of calculated formation enthalpies in the absence of experimental information.

Selecting the more appropriate ε_{xc} is less clear for calculation of the elasticity tensor components C_{ij}. While the GGA yields better overall agreement with experiment for Ca, Sr, and Ba metals, our results for Be and Mg show that one ε_{xc} is preferable for the diagonal elements C_{ii} while the other provides better accord with data for $C_{i\neq j}$. Measurements of the elastic constants for the hydrides are certainly desirable for further investigation of this issue.

APPENDIX: $E_{ZPE}(V)$

In principle, both the electronic total energy E_{el} and the zero point energy E_{ZPE} should be calculated as functions of the cell volume V (or, preferably, the lattice constants in the

TABLE XIII. Volumes V_{el}^0 and V_{el+ZPE}^0 that minimize $E_{el}(V)$ and $[E_{el}(V)+E_{ZPE}(V)]$, respectively, in the GGA for Be and BeH_2.

		Be	BeH_2
V_{el}^0/V_{expt}		0.977	0.965
V_{el+ZPE}^0/V_{expt}		0.996	1.029
$E_{el}(V)+E_{ZPE}(V)$	$V=V_{el+ZPE}^0$	−349.1	−987.2
(kJ/mol f.u.)	$V=V_{el}^0$	−349.0	−987.2

case of noncubic systems) and $[E_{el}(V)+E_{ZPE}(V)]$, rather than $E_{el}(V)$ alone, minimized to derive the zero temperature lattice parameters. This may be significant for materials having a substantial mass fraction of light elements, but it is much more demanding computationally since the phonon spectra needed to obtain $E_{ZPE}(V)$ must be computed for a series of volumes. Figures 6 and 7 present the results of such calculations for Be and BeH_2 in the GGA. We see from Figs. 6(a) and 7(a) that $E_{ZPE}(V)$ (i) is ~3% (~5%) of $E_{el}(V)$ for Be (BeH_2) and (ii) decreases monotonically with V, reflecting similar behavior of the interionic interactions. We fit $E_{el}(V)$ and $[E_{el}(V)+E_{ZPE}(V)]$, displayed in Figs. 6(b) and 7(b), with the Birch-Murnaghan equation of state[100] to obtain the volumes V^0_{el} and V^0_{el+ZPE} minimizing each; results are given in Table XIII. In both cases, the inclusion of $E_{ZPE}(V)$ increases the computed 0 K cell volume. The enhancement is 1.9% for Be and improves the agreement with experiment. The corresponding increase for BeH_2 is 6.6%, with V^0_{el} underestimating V_{expt} by 3.5% and V^0_{el+ZPE} overestimating it by 2.9%. ZPE-corrected lattice constants, estimated from V^0_{el+ZPE} by assuming the experimental ratios, are included in Table I (Table IV) for Be (BeH_2).

Table XIII also lists $[E_{el}(V)+E_{ZPE}(V)]$ evaluated at V^0_{el+ZPE} and V^0_{el}. The difference between the two values is at most 0.1 kJ/mol f.u., demonstrating that $E_{ZPE}(V)$ has negligible impact on the total energy and, hence, formation enthalpies ΔH. That is, computing E_{ZPE} at the single volume V^0_{el} which minimizes $E_{el}(V)$ and neglecting its volume dependence is quite sufficient to derive precise ΔH. We found similar results for cubic LiH previously.[101] Inclusion of $E_{ZPE}(V)$ expands the lattice constant from 4.00 to 4.09 Å in the GGA, but $[E_{el}(V)+E_{ZPE}(V)]$ changes by only 0.4 kJ/mol LiH.

[1] F. E. Pinkerton and B. G. Wicke, Ind. Phys. **10**, 20 (2004).
[2] J. P. Tessier, J. Huot, R. Schulz, and D. Guay, J. Alloys Compd. **376**, 180 (2004).
[3] P. S. Rudman and G. D. Sandrock, Annu. Rev. Mater. Sci. **12**, 271 (1982).
[4] K. H. J. Buschow, in *Handbook on the Physics and Chemistry of Rare Earths*, edited by K. A. Gschneidner, Jr. and L. Eyring (North-Holland, Amsterdam, 1984), Vol. 6, p. 1.
[5] W. Kohn and L. Sham, Phys. Rev. **140**, A1133 (1965).
[6] H. Smithson, C. A. Marianetti, D. Morgan, A. Van der Ven, A. Predith, and G. Ceder, Phys. Rev. B **66**, 144107 (2002).
[7] C. Wolverton, V. Ozolins, and M. Asta, Phys. Rev. B **69**, 144109 (2004).
[8] R. M. Martin, *Electronic Structure: Basic Theory and Practical Methods* (Cambridge University Press, New York, 2004).
[9] R. Yu and P. K. Lam, Phys. Rev. B **37**, 8730 (1988).
[10] N. Ohba, K. Miwa, T. Noritake, and A. Fukumoto, Phys. Rev. B **70**, 035102 (2004).
[11] Y. Song, Z. X. Guo, and R. Yang, Phys. Rev. B **69**, 094205 (2004).
[12] G. Liang, J. Huot, S. Boily, A. Van Neste, and R. Schulz, J. Alloys Compd. **292**, 247 (1999).
[13] D. Chen, Y. M. Wang, L. Chen, S. Liu, C. X. Ma, and L. B. Wang, Acta Mater. **52**, 521 (2004).
[14] J. F. R. de Castro, A. R. Yavari, A. LeMoulec, T. T. Ishikawa, and W. J. Botta, J. Alloys Compd. **389**, 270 (2005).
[15] H. Imamura, J. Less-Common Met. **172**, 1064 (1991).
[16] H. Imamura, N. Sakasai, and T. Fujinaga, J. Alloys Compd. **253-254**, 34 (1997).
[17] A. Zaluska, L. Zaluski, and J. O. Ström-Olsen, J. Alloys Compd. **289**, 197 (1999).
[18] J. Huot, G. Liang, S. Boily, A. Van Neste, and R. Schulz, J. Alloys Compd. **293-295**, 495 (1999).
[19] E. Wachowicz and A. Kiejna, J. Phys.: Condens. Matter **13**, 10767 (2001).
[20] G. Kresse and J. Hafner, Phys. Rev. B **49**, 14251 (1994).
[21] G. Kresse and J. Furthmüller, Comput. Mater. Sci. **6**, 15 (1996).
[22] P. E. Blöchl, Phys. Rev. B **50**, 17953 (1994).
[23] G. Kresse and D. Joubert, Phys. Rev. B **59**, 1758 (1999).
[24] D. M. Ceperley and B. J. Alder, Phys. Rev. Lett. **45**, 566 (1980).
[25] J. P. Perdew and A. Zunger, Phys. Rev. B **23**, 5048 (1981).
[26] J. P. Perdew and Y. Wang, Phys. Rev. B **45**, 13244 (1992).
[27] J. P. Perdew, J. A. Chevary, S. H. Vosko, K. A. Jackson, M. R. Pederson, D. J. Singh, and C. Fiolhais, Phys. Rev. B **46**, 6671 (1992).
[28] S. H. Vosko, L. Wilk, and M. Nusair, Can. J. Phys. **58**, 1200 (1980).
[29] W. H. Press, S. A. Teukolsky, W. T. Vetterling, and B. P. Flannery, *Numerical Recipes in FORTRAN 90: The Art of Parallel Scientific Computing*, 2nd ed. (Cambridge University Press, New York, 1996).
[30] H. J. Monkhorst and J. D. Pack, Phys. Rev. B **13**, 5188 (1976).
[31] P. E. Blöchl, O. Jepsen, and O. K. Andersen, Phys. Rev. B **49**, 16223 (1994).
[32] K. Parlinski, Software Phonon 3.11, Cracow, as implemented in MedeA 1.8, Materials Design, Le Mans, France and Taos, NM (www.MaterialsDesign.com).
[33] G. Kresse, J. Furthmüller, and J. Hafner, Europhys. Lett. **32**, 729 (1995).
[34] K. Parlinski, Z-. Q. Li, and Y. Kawazoe, Phys. Rev. Lett. **78**, 4063 (1997).
[35] K. Parlinski, J. Lazewski, and Y. Kawazoe, J. Phys. Chem. Solids **61**, 87 (2000).
[36] S. Baroni, S. de Gironcoli, A. Dal Corso, and P. Giannozzi, Rev. Mod. Phys. **73**, 515 (2001).
[37] M. Methfessel and A. T. Paxton, Phys. Rev. B **40**, 3616 (1989).
[38] R. M. Pick, M. H. Cohen, and R. M. Martin, Phys. Rev. B **1**, 910 (1970).
[39] See LEPSILON: static dielectric matrix using density functional perturbation theory. http://cms.mpi.univie.ac.at/vasp/vasp/node159.html
[40] R. D. King-Smith and D. Vanderbilt, Phys. Rev. B **47**, 1651 (1993).
[41] D. Vanderbilt and R. D. King-Smith, Phys. Rev. B **48**, 4442 (1993).
[42] See Berry phase calculations. http://cms.mpi.univie.ac.at/vasp/vasp/node139.html

[43] Y. Le Page and P. Saxe, Phys. Rev. B **65**, 104104 (2002).
[44] J. R. Gladden, J. H. So, J. D. Maynard, P. W. Saxe, and Y. Le Page, Appl. Phys. Lett. **85**, 392 (2004).
[45] L. G. Hector, Jr., J. F. Herbst, and T. W. Capehart, J. Alloys Compd. **353**, 74 (2003).
[46] L. G. Hector, Jr. and J. F. Herbst, J. Alloys Compd. **379**, 41 (2004).
[47] R. Stadler, W. Wolf, R. Podloucky, G. Kresse, J. Furthmüller, and J. Hafner, Phys. Rev. B **54**, 1729 (1996).
[48] The $E(H_2)=-6.8016$ eV GGA result differs slightly from the −6.795 eV value we reported in Ref. 45, which was obtained with a 700 eV cutoff in a $(9\ \text{Å})^3$ box.
[49] W. Kolos and C. C. J. Roothaan, Rev. Mod. Phys. **32**, 219 (1960).
[50] J. Paier, R. Hirschl, M. Marsman, and G. Kresse, J. Chem. Phys. **122**, 234102 (2005).
[51] V. Vijayakumar, B. K. Godwal, Y. K. Vohra, S. K. Sikka, and R. Chidambaram, J. Phys. F: Met. Phys. **14**, L65 (1984).
[52] F. Jona and P. M. Marcus, J. Phys.: Condens. Matter **15**, 7727 (2003).
[53] V. A. Sashin, M. A. Bolorizadeh, A. S. Kheifets, and M. J. Ford, J. Phys.: Condens. Matter **13**, 4203 (2001).
[54] S. K. Reed and G. J. Ackland, Phys. Rev. Lett. **84**, 5580 (2000).
[55] J. A. Moriarty, Phys. Rev. B **28**, 4818 (1983).
[56] G. M. Wang, D. A. Papaconstantopoulos, and E. Blaisten-Barojas, J. Phys. Chem. Solids **64**, 185 (2003).
[57] M. Heiroth, U. Buchenau, H. R. Schober, and J. Evers, Phys. Rev. B **34**, 6681 (1986).
[58] J. E. Hearn, R. L. Johnston, S. Leoni, and J. N. Murrell, J. Chem. Soc., Faraday Trans. **92**, 425 (1996).
[59] J. Mizuki and C. Stassis, Phys. Rev. B **32**, 8372 (1985).
[60] S. A. Canney, V. A. Sashin, M. J. Ford, and A. S. Kheifets, J. Phys.: Condens. Matter **11**, 7507 (1999).
[61] R. E. DeWames, T. Wolfram, and G. W. Lehman, Phys. Rev. **138**, A717 (1965).
[62] X. M. Chen, Y. Xuan, and A. W. Overhauser, Phys. Rev. B **43**, 1799 (1991).
[63] J.-P. Jan and H. L. Skriver, J. Phys. F: Met. Phys. **11**, 805 (1981).
[64] P. Blaha and J. Callaway, Phys. Rev. B **32**, 7664 (1985).
[65] B. Vasvari, A. O. E. Animalu, and V. Heine, Phys. Rev. **154**, 535 (1967).
[66] N. Singh and S. P. Singh, Phys. Status Solidi B **158**, 433 (1990).
[67] W.-S. Zeng, V. Heine, and O. Jepsen, J. Phys.: Condens. Matter **9**, 3489 (1997).
[68] J. S. Ononiwu, Can. J. Phys. **76**, 143 (1998).
[69] Y. W. Yang and P. Coppens, Acta Crystallogr., Sect. A: Cryst. Phys., Diffr., Theor. Gen. Crystallogr. **A34**, 61 (1978).
[70] G. V. Raynor, Proc. R. Soc. London, Ser. A **174**, 457 (1940).
[71] J. C. Schottmiller, A. J. King, and F. A. Kanda, J. Phys. Chem. **62**, 1446 (1958).
[72] R. G. Hirst, A. J. King, and F. A. Kanda, J. Phys. Chem. **60**, 302 (1956).
[73] J. Phys. Chem. Ref. Data Monogr. No. 9, NIST-JANAF Thermochemical Tables, edited by Malcolm W. Chase (American Institute of Physics, Woodbury, NY, 1998).
[74] N. A. W. Holzwarth and Y. Zeng, Phys. Rev. B **51**, 13653 (1995).
[75] W. F. King and P. H. Cutler, Phys. Lett. **28A**, 289 (1968).
[76] L. F. Magaña and G. J. Vázquez, J. Phys.: Condens. Matter **7**, L393 (1995).
[77] L. Dagens, J. Phys. F: Met. Phys. **7**, 1167 (1977).
[78] S. Das and A. Sarkar, Pramana **28**, 689 (1987).
[79] G. Simmons and H. Wang, *Single Crystal Elastic Constants and Calculated Aggregate Properties: A Handbook*. (M.I.T. Press, Cambridge, MA, 1971).
[80] A. Migliori, H. Ledbetter, D. J. Thoma, and T. W. Darling, J. Appl. Phys. **95**, 2436 (2004).
[81] C. Stassis, J. Zaretsky, D. K. Misemer, H. L. Skriver, B. N. Harmon, and R. M. Nicklow, Phys. Rev. B **27**, 3303 (1983).
[82] U. Buchenau, M. Heiroth, H. R. Schober, J. Evers, and G. Oehlinger, Phys. Rev. B **30**, 3502 (1984).
[83] K. A. Gschneidner, Jr., Solid State Phys. **16**, 275 (1964).
[84] S. N. Vaidya and G. C. Kennedy, J. Phys. Chem. Solids **31**, 2329 (1970).
[85] G. Grimvall, *Thermophysical Properties of Materials* (Elsevier, Amsterdam, 1999).
[86] G. S. Smith, Q. C. Johnson, D. K. Smith, D. E. Cox, R. L. Snyder, R.-S. Zhou, and A. Zalkin, Solid State Commun. **57**, 491 (1988).
[87] P. Vajeeston, P. Ravindran, A. Kjekshus, and H. Fjellvåg, Appl. Phys. Lett. **84**, 34 (2004).
[88] R. Yu, P. K. Lam, and J. Head, Solid State Commun. **70**, 1043 (1989).
[89] P. Vajeeston, P. Ravindran, A. Kjekshus, and H. Fjellvåg, Phys. Rev. Lett. **89**, 175506 (2002).
[90] A. El Gridani and M. El Mouhtadi, Chem. Phys. **252**, 1 (2000).
[91] A. El Gridani, R. D. El Bouzaidi, and M. El Mouhtadi, J. Mol. Struct. **531**, 193 (2000).
[92] A. El Gridani, R. D. El Bouzaidi, and M. El Mouhtadi, J. Mol. Struct. **577**, 161 (2002).
[93] W. H. Zachariasen, C. E. Holley, Jr., and J. F. Stamper, Jr., Acta Crystallogr. **16**, 352 (1963).
[94] T. Sichla and H. Jacobs, Eur. J. Solid State Inorg. Chem. **33**, 453 (1996).
[95] W. Bronger, S. Chi-Chien, and P. Müller, Z. Anorg. Allg. Chem. **545**, 69 (1987).
[96] F. H. Ellinger, C. E. Holley, Jr., B. B. McInteer, D. Pavone, R. M. Potter, E. Staritzky, and W. H. Zachariasen, J. Am. Chem. Soc. **77**, 2647 (1955).
[97] J. Bergsma and B. O. Loopstra, Acta Crystallogr. **15**, 92 (1962).
[98] E. Zintl and A. Harder, Z. Elektrochem. Angew. Phys. Chem. **41**, 33 (1935).
[99] G. J. Snyder, H. Borrmann, and A. Simon, Z. Kristallogr. **209**, 458 (1994).
[100] F. Birch, Phys. Rev. **71**, 809 (1947).
[101] J. F. Herbst and L. G. Hector, Jr., Phys. Rev. B **72**, 125120 (2005).
[102] M. Gajdos, K. Hummer, G. Kresse, J. Furthmüller, and F. Bechstedt, Phys. Rev. B **73**, 045112 (2006).
[103] J. P. Perdew, K. Burke, and M. Ernzerhof, Phys. Rev. Lett. **77**, 3865 (1996).
[104] M. H. Brodsky and E. Burstein, J. Phys. Chem. Solids **28**, 1655 (1967).
[105] D. K. Blat, N. E. Zein, and V. I. Zinenko, J. Phys.: Condens. Matter **3**, 5515 (1991).
[106] J. R. Santisteban, G. J. Cuello, J. Dawidowski, A. Fainstein, H. A. Peretti, A. Ivanov, and F. J. Bermejo, Phys. Rev. B **62**, 37 (2000).
[107] G. N. García, J. P. Abriata, and J. O. Sofo, Phys. Rev. B **59**, 11746 (1999).
[108] W. R. Myers, L.-W. Wang, T. J. Richardson, and M. D. Rubin, J. Appl. Phys. **91**, 4879 (2002).

[109] L. G. Hector, Jr. and J. F. Herbst, J. Alloys Compd. **379**, 41 (2004).
[110] S. M. Opalka and D. L. Anton, J. Alloys Compd. **356-357**, 486 (2003).
[111] M. D. Senin, V. V. Akhachinskii, Y. E. Markushkin, N. A. Chirin, L. M. Kopytin, I. P. Mikhalenko, N. M. Ermolaev, and A. V. Zabrodin, Inorg. Mater. **29**, 1416 (1993).
[112] *Metal Hydrides*, edited by W. M. Mueller, J. P. Blackledge, and G. G. Libowitz (Academic Press, New York, 1968).
[113] *CRC Handbook of Chemistry and Physics*, 80th ed., edited by D. R. Lide (CRC Press, Boca Raton, 1999).
[114] G. Herzberg, *Molecular Spectra and Molecular Structure, I. Diatomic Molecules* (Prentice-Hall, New York, 1939).
[115] I. Baraille, C. Pouchan, M. Causa, and C. Pisani, Chem. Phys. **179**, 39 (1994).
[116] C. Kittel, *Introduction to Solid State Physics*, 7th ed. (Wiley, New York, 1996).
[117] Y. Qi and L. G. Hector, Jr., Phys. Rev. B **69**, 235401 (2004).
[118] M. Born and H. Huang, *Dynamical Theory of Crystal Lattices* (Clarendon Press, Oxford, 1954).
[119] S. Yip, J. Li, M. Tang, and J. Wang, Mater. Sci. Eng., A **317**, 236 (2001).